Manuscript number: RSTA-2012-0335

On the nucleation of dust in oxygen-rich stellar outflows

John M. C. Plane

School of Chemistry

University of Leeds

Leeds LS2 9JT

United Kingdom.

Philosophical Transactions A

Issue on **Surface Science in the Interstellar Medium**

Published as Phil Trans R Soc A 371: 20120335.

http://dx.doi.org/10.1098/rsta.2012.0335

Abstract

Understanding the nature of dust condensation in the outflow from oxygen-rich AGB stars is a continuing problem. A kinetic model has been developed to describe the formation of gas-phase precursors from Ca, Mg, Fe, SiO and TiO in an outflow cooling from 1500 to 1000 K. Electronic structure calculations are used to identify efficient reaction pathways which lead to the formation of metal titanates and silicates. The molecular properties of the stationary points on the relevant potential energy surfaces are then used in a multi-well master equation solver to calculate pertinent rate coefficients. The outflow model couples an explicit treatment of gas-phase chemistry to a volume-conserving particle growth model. $CaTiO_3$ is shown to be the overwhelming contributor to the formation of condensation nuclei (CN), with less than 0.01% provided by $CaSiO_3$, $(TiO_2)_2$ and $FeTiO_3$. Magnesium species make a negligible contribution. Defining CN as particles with radii greater than 2 nm, the model shows that for stellar mass loss rates above 3×10^{-5} $M_\odot$ y^{-1} more than 10^{-13} CN per H nucleus will be produced when the outflow temperature is still well above 1000 K. This is sufficient to explain the observed number density of grains in circumstellar dust shells.

Keywords: AGB star, circumstellar dust, calcium titanate

Introduction

Mass loss from stars is fundamental to the chemical evolution of galaxies. During the late stages of stellar evolution, asymptotic giant branch (AGB) stars with masses between about 1 and 8 $M_{\odot}$ lose a significant fraction of their mass in a short period, during which they are surrounded by an optically thick shell of dust [1]. This circumstellar dust plays a crucial role in many astrophysical processes: it dominates the energy balance around the star through the absorption and emission of radiation, so that the resulting radiation pressure induces a massive acceleration in the outflow velocity; it is a significant source of interstellar dust particles which provide the surfaces on which heterogeneous chemical synthesis can occur; and finally the dust is involved in the formation of new planets around young stars.

Spectroscopic observations of circumstellar dust reveal broad emission features at about 10 and 18 μm in the IR, as well as features in the far-IR between 30 and 44 μm, indicating that major components of the dust are amorphous magnesium-iron-silicates (olivine and pyroxene) [2,3]. This paper is concerned with the nature of the condensation nuclei (CN) or "seeds" on which the relatively abundant species Mg, Fe and SiO subsequently condense from the gas phase, once the outflow has cooled sufficiently, to form these metal silicates [4]. This condensation causes the CN particles, initially only about 1 nm in radius, to grow to their observed size of several hundred nm [5]. It is crucially important to understand the composition of CN and how they form, in order to predict their size distribution in the outflow and hence the likely number density of dust particles which subsequently enter the interstellar medium.

The CN particles must be highly refractory, since the inner edge of observable dust clouds is typically at the point where the temperature in the outflow is still above 1000 K, at a distance

of about $4R_*$ from the star (R_* is the star radius, which is around 1 AU for an AGB star). Such observations imply that the CN have formed at higher temperatures, most likely in the region between $3R_*$ and $4R_*$ where the temperature decreases from ~1200 to 1000 K [6]. In spite of these high temperatures, CN can form because the relatively high pressures facilitate recombination (or association) reactions between individual molecules, which must be the starting point for CN synthesis and eventual dust production.

There are several reasons why this is a challenging environment in which to form new particles from the gas-phase constituents which are present in the outflow. Firstly, molecules need to be very stable to survive thermal dissociation, which requires that their bond energies are greater than 400 kJ mol^{-1}. Secondly, the major constituent of the outflow is H_2, with about 1 part in 10^3 being H_2O. Since OH is observed around circumstellar shells [7], this implies that there must also be significant quantities of H atoms in steady state with H_2 and H_2O (the H/OH ratio will be ~10^5). Both H and H_2 are chemically reducing species, which prevent the oxidation of metals and silicon oxides (see below).

Thirdly, the total pressure in the stellar outflow is very low, only around 0.01 Pa at $3R_*$ for a high stellar mass loss rate [8]. This has the effect of slowing down the rates of any recombination reactions (i.e. A + B + M $\rightarrow$ AB + M), which are pressure dependent because the "third body" M is required to stabilise the products. Finally, the formation of more complex gas-phase species from species such as Mg, Fe and SiO involves reactions between at least two constituents in the outflow; the rates of these reactions will therefore have at least a second-order dependence on the total density in the outflow, and decrease rapidly as the flow expands away from the star.

Gail, Sedlmayr and their co-workers have published extensively on possible candidates for CN production. They showed that the direct nucleation of Mg, Fe and SiO from the gas phase was very unlikely at temperatures above 1000 K [4,9,10], and therefore considered less

abundant but more refractory alternatives in an O-rich stellar outflow, including Fe, TiO_2, SiO_2, SiO, TiO and Al_2O_3. They concluded that only TiO_2 provided a nucleation rate in the range required to account for the observed dust density in circumstellar dust shells [6]. Nevertheless, there is continuing debate about whether SiO itself can condense, perhaps enhanced by the presence of Fe and Mg [11,12].

Previous workers have generally addressed the dust formation problem using homogeneous classical nucleation theory (CNT) to estimate the nucleation rate (J_*). CNT determines a Gibbs free energy barrier at a critical cluster size (typically about 20 monomers), after which runaway growth occurs [9]. The barrier arises from competition between the favourable binding energies of successive monomers to the embryonic cluster, and an unfavourable increase in the interfacial surface energy. The steady-state concentration of critical clusters (which assumes chemical equilibrium) is then multiplied by the rate of addition of a further monomer to estimate J_*. There are a number of difficulties with CNT, including the fact that the circumstellar environment is not in a local chemical equilibrium, and that the bulk thermodynamic properties and surface tension of the condensed phase which are required to calculate J_* may well not be applicable at the cluster size-scale. Nuth and co-workers were initially rather critical of CNT for these reasons [13], although very recently they have shown that the lack of chemical equilibrium is perhaps not such a serious problem [14]. These workers have also introduced a scaled version of CNT [12]. Cherchneff and Dwek [15] have also recently discussed the shortcomings of CNT in some detail. As an alternative to CNT, those authors have developed a kinetic model describing explicitly the formation in the gas phase of the molecular precursors which polymerise to form embryonic dust particles.

The present study follows a similar strategy. The starting point is our recent experimental work on the formation of mixed Mg-Fe-silicate particles at low temperatures from gas-phase precursors [16], related to the formation of nanoparticles from ablated meteor vapours in the

earth's upper atmosphere [17,18]. We interpreted the laboratory observations using electronic structure calculations to show that $FeSiO_3$ and $MgSiO_3$ molecules should play a central role in forming new particles. These molecules are very stable and highly polar (see below), so that they should polymerise spontaneously to form particles. For this reason they have not (yet) been observed in the laboratory, although we have studied the formation in the gas phase of their close analogues $FeCO_3$, $MgCO_3$ and $CaCO_3$, from the recombination of the respective metal oxides with CO_2 [19,20,21].

The kinetic approach used here to model particle formation in stellar outflows involves three stages. First, electronic structure calculations are used to determine energetically possible reaction pathways. Second, the molecular properties (rotational constants and vibrational frequencies) of stable intermediates and transition states are then used to calculate reaction rates over typically complex potential energy surfaces. Third, the resulting rate coefficients are employed in a model which couples gas-phase chemistry with particle growth kinetics in a stellar outflow. This model demonstrates that silicate formation in the gas phase is essentially shut down by the presence of atomic H in the outflow. However, there is a kinetically viable route to the formation of gas-phase $CaTiO_3$, and this molecule is probably the key ingredient in forming sufficient numbers of CN particles larger than 2 nm by the point at which the outflow has cooled to 1000 K.

Theoretical Methods

Electronic structure calculations and master equation modelling

Electronic structure calculations were used to map the stationary points on the electronic potential energy surfaces (PESs) of the relevant reactions. Molecular geometries were first

optimised using hybrid density functional theory, which includes some exact Hartree-Fock exchange. The B3LYP method was used together with the 6-311+G(2d,p) triple zeta basis set. This is a large, flexible basis set which has both polarization and diffuse functions added to the atoms. At this level of theory, previous theoretical benchmarking studies indicate an expected uncertainty in the calculated reaction enthalpies on the order of ±25 kJ mol^{-1} [22]. After the optimised geometries were checked for wavefunction stability, the resulting rotational constants and vibrational frequencies were used in the master equation calculations described below. More accurate energies (± 15 kJ mol^{-1} [22]) were then determined using the *Complete Basis Set* (CBS-Q) method of Petersson and co-workers [23]. All calculations were performed using the Gaussian 09 suite of programs [24].

Reaction rate coefficients were then estimated using Rice-Ramsperger-Kassel-Markus (RRKM) theory, employing a solution of the master equation (ME) based on the inverse Laplace transform method [25]. We have previously used this method to model successfully the measured rate coefficients of reactions involving metal-containing species where a stable intermediate is present on the potential energy surface (PES) [19,20,21,26]. These reactions proceed via the formation of an excited adduct from the two reactants. This adduct can then dissociate back to reactants, rearrange to other intermediates, or dissociate to bimolecular products. Any of the intermediates can also be stabilized by collision with the third body. The time evolution of all these possible outcomes is modelled using the ME.

For this study, a multiwell energy-grained master equation was used [27,28,29]. The internal energies of the intermediates on the PES were divided into a contiguous set of grains (width 200 cm^{-1}), each containing a bundle of rovibrational states. Each grain was then assigned a set of microcanonical rate coefficients linking it to other intermediates, calculated by RRKM theory. For dissociation to products or reactants, microcanonical rate coefficients were determined using inverse Laplace transformation to link them directly to the capture rate

coefficient, $k_{capture}$. For these reactions involving neutral species, $k_{capture}$ was set to a typical capture rate coefficient of 3×10^{-10} $(T/1000\ K)^{1/6}$ cm^3 $molecule^{-1}$ s^{-1} [30], where the small positive temperature dependence is characteristic of a long-range potential governed by dispersion and ion-induced dipole forces. For reactions governed by permanent dipole-dipole interactions (e.g. SiO + OH), the capture rate was calculated explicitly using long-range variational transition state theory [30].

The probability of collisional transfer between grains was estimated using the exponential down model, where the average energy for downward transitions was set to $<\Delta E>_{down} = 300$ cm^{-1} [31]. The probabilities for upward transitions were calculated by detailed balance. All RRKM and ME calculations reported in this study were carried out with the open source master equation program, MESMER (Master Equation Solver for Multi-well Energy Reactions) [32]. MESMER determines the temperature- and pressure-dependent rate coefficient from the full microcanonical description of the system time evolution by performing an eigenvector/eigenvalue analysis similar to that described by Bartis and Widom [27,28,33].

Model of stellar outflow chemistry

The rate coefficients obtained from the procedures described above were then input into a chemical box model where the coupled ordinary differential equations describing the rates of change of the concentrations of each species were solved using a 4^{th}-order Runge Kutta integrator [34]. In addition to the reactions involving Ca, Fe, Mg, Ti and Si species, the model also contained a full set of odd-hydrogen reactions (i.e. involving the radicals H and OH) whose rate coefficients are well known from combustion chemistry [35].

The model was initialised with the following conditions. The AGB star has a radius of 200 $R_\odot$ = 1.4 × 10^8 km, close to 1 AU. The mass loss rate was varied from (2 – 10) × 10^{-5} $M_\odot$ y^{-1} [36]. This range corresponds to an H_2 loss rate of (4 – 20) × 10^{44} molecules s^{-1}. The mass continuity equation for a stationary spherically symmetric outflow is given by

$$\frac{dM}{dt} = 4\pi R^2 v[\mathrm{H}_2] \qquad \text{(I)}$$

where v is the outflow velocity which was fixed in the model at 2 km s^{-1} [8]. That is, it is assumed that the gas enters the zone of condensation of the main components (Mg, Fe, SiO) with roughly sonic velocity, and acceleration of the dust outflow only occurs after the dust grows to a size where radiation pressure becomes dynamically significant [4]. The H_2 concentration at $2R_*$ then ranges from (1.0 – 10.3) × 10^{11} cm^{-3} depending on the H_2 loss rate, and falls as $1/R^2$. The temperature T at $2R_*$ was taken as 1600 K, and was assumed to decrease according to the relation [8]

$$T = 1600\left(\frac{2R_*}{R}\right)^{0.7} \qquad \text{(II)}$$

reaching ~1000 K at $4R_*$.

The relative elemental abundances were set to their cosmic abundances [37]. Assuming that all C is oxidised to CO, then excess O should almost all be in the form of H_2O. The model was then initialised with the following relative abundances (in parentheses): H_2 (1.0), H_2O (1.7 × 10^{-3}), Mg (7.9 × 10^{-5}), SiO (7.1 × 10^{-5}), Fe (6.4 × 10^{-5}), Ca (4.4 × 10^{-6}) and TiO (1.7 × 10^{-7}). It should be noted that the relative abundances of the metallic species compared to hydrogen agree to better than 1% with a recent compilation of elemental abundances in the solar photosphere [38]; although the relative abundances of silicon, oxygen and carbon are 8, 18 and 23% smaller, respectively, this is not important for the present modelling exercise.

The H relative abundance was fixed (arbitrarily) to 2×10^{-3} (i.e. 0.1% of the H_2 is dissociated), and the OH concentration was calculated from the odd-H chemistry in the model. The OH relative abundance then varied from 7.1×10^{-8} at 1500 K to 5×10^{-9} at 1000 K. In fact, the choice of H relative abundance in the model is not critical (over a sensible range) because the OH/H ratio is largely controlled by the reaction $OH + H_2 \rightarrow H_2O + H$ and its reverse $H_2O + H \rightarrow OH + H_2$. Although the latter is slower, its time constant is still only ~ 2 days (at 1200 K and $[H_2O] = 3 \times 10^8$ cm^{-3}), which is much shorter than the characteristic timescale during which CN form in the outflow (> 100 days, see below). Thus, the OH/H ratio is essentially governed by the H_2O/H_2 ratio. The OH/H ratio in turn controls the ratios of TiO_2/TiO and SiO_2/SiO (see below), so that all these species exist in near steady state.

The gas-phase part of the outflow model was then coupled to a particle growth model which we have described in detail previously [17]. The growth model, which uses a semi-implicit integration scheme, is volume-conserving. Particle sizes are separated into radius space in a number of fixed centre bins, where the first bin size is set at an appropriate molecular radius of 2.8 nm, corresponding to the equivalent size of a spherical monomer of $CaTiO_3$ (since this turns out to be the dominant condensable molecule) with an assumed amorphous density of 2500 kg m^{-3}. Subsequent bin sizes are increased geometrically by a fixed volume ratio of 1.5, so that the particle radius in each successive bin is $(1.5)^{1/3}$ times larger, and the largest of the 45 bins contains particles of radius 106 nm. The concentration of monomers in the first bin is set equal to the concentration of gas-phase metal silicates and titanates at each time step of the gas-phase module.

Particle growth is assumed to be dominated by Brownian diffusion-coagulation where collisions between pairs of particles result in coalescence, maintaining spherical morphology and compact structure. The collision rate coefficients (or kernels) for Brownian coagulation were calculated using the Fuchs interpolation formula [39] for the transition regime (Knudsen

number, K_n ~ 1). However, the kernel for the dimerisation of two monomers (i.e. to move from the first to second bin) was calculated explicitly using the MESMER code. It is assumed that polymerisation to larger polymers is no longer pressure-dependent because of the increasing numbers of atoms involved, which give rise to a large number of vibrational modes and a correspondingly large density of rovibrational states at the critical energy [31].

We have used this growth model previously to treat the agglomerative growth of fractal-like particles, in particular where the rapid growth of Fe-containing particles is driven by magnetic dipoles once they reach a primary particle radius around 4 nm [40]. However, these factors were not considered in the present study, firstly because the CN particles under consideration only reach a few nm in size, and secondly because the fraction of Fe in the particles is very low (< 0.01%, see below).

Results and Discussion

Figure 1 illustrates the reaction pathway to form $CaTiO_3$ and its dimer, $(CaTiO_3)_2$, from Ca and TiO. This mechanism, which has been elucidated using the theoretical and modelling tools described above, appears to be a key reaction sequence for CN formation in an oxygen-rich stellar outflow. Various aspects of the mechanism are discussed in the sections below. Electronic structure calculations reveal that the metal silicate and titanate molecules are kite-shaped molecules. The silicates are planar [18], whereas the titanates are pyramidal, as shown for the case of $CaTiO_3$ at the bottom of Figure 1. These molecules possess several essential properties required to act as effective building blocks of CN particles at high temperatures. Firstly, as shown in Table 1, the molecules are extremely stable with respect to thermal dissociation, particularly $CaTiO_3$ and $CaSiO_3$. In all cases, the lowest energy thermal

dissociation pathway yields the metal oxide and TiO_2 or SiO_2 e.g. $CaTiO_3 \rightarrow CaO + TiO_2$, which is endothermic by 585 kJ mol^{-1}. Secondly, reactions with atomic H must be slow because they are quite endothermic e.g. for the reaction $CaTiO_3 + H \rightarrow CaOH + TiO_2$, ΔH = 148 kJ mol^{-1}. This means that these molecules will have a chance to survive long enough, at high temperatures and in the presence of significant H atom concentrations, to polymerise and form particles.

Thirdly, the molecules have extremely high dipole moments (Table 1), some in excess of 10 Debye. This means that there will be strong dipole-dipole forces between them, resulting in unusually high capture rates [30]. For instance, the capture rate for the dimerisation reaction $CaTiO_3 + CaTiO_3$ is 9.1×10^{-10} cm^3 $molecule^{-1}$ s^{-1} at 1000 K, which is about a factor of 3 larger than the "hard-sphere" collision rate. A final point is that these molecules polymerise readily, with binding energies in excess of the lower limit of 400 kJ mol^{-1} required for reasonable thermal stability at a temperature around 1000 K.

Having established that these molecules should be effective building blocks, the question is whether they can actually form in this challenging environment of high temperatures, low pressures, and chemically reducing atomic H and H_2.

Oxidation of Mg, Fe and Ca

The oxidation of metal atoms to form metal monoxides or hydroxides (MgO, MgOH etc.), as precursors to titanates and silicates, is effectively shut down by H_2 and H. For example, we have shown experimentally that the reaction

$$CaO + H_2 \rightarrow Ca + H_2O \qquad \Delta H_0 = -79 \text{ kJ mol}^{-1} \qquad (1)$$

is close to the collision frequency even at room temperature [41]. The PES for $MgO + H_2$ indicates that this reaction should also be rapid. This probably explains why neither CaO nor

MgO have been identified in circumstellar environments [42]. We measured a small upper limit at room temperature for the reaction FeO + H_2, $k \leq 7 \times 10^{-14}$ cm^3 $molecule^{-1}$ s^{-1} [19]. This is consistent with a potential energy barrier of 55 kJ mol^{-1} calculated at the CBS-Q level, yielding k(FeO + H_2) = 6.2×10^{-11} exp(-7970/T) cm^3 $molecule^{-1}$ s^{-1}. At an H_2 pressure of 10^{-3} Pa and a temperature of 1000 K, the lifetime of FeO will be only 700 s. This may account for the single report so far of FeO in the circumstellar medium [43].

The reactions of the metal oxides and hydroxides with atomic H are all exothermic. The reaction FeOH + H $\rightarrow$ Fe + H_2O is fast even at room temperature [26], and flame studies show that CaOH + H and MgOH + H are within an order of magnitude of their respective collision frequencies [44,45]. It therefore appears very unlikely that metal titanates and silicates can form in the outflow region via direct oxidation of the metal atoms.

Oxidation of TiO and SiO

We have recently measured the kinetics of the reaction

$$SiO + OH \rightarrow SiO_2 + H \qquad \Delta H_0 = -6 \text{ kJ mol}^{-1} \qquad (2)$$

obtaining k_2(293 K) = $(5.7 \pm 2.0) \times 10^{-12}$ cm^3 $molecule^{-1}$ s^{-1} [46]. In the same study we computed the PES for the reaction: this is quite complex because of the initial formation of a *cis* or *trans* form of the HOSiO intermediate, which then rearranges in different ways to yield the products. Figure 2 shows a plot of the temperature dependence of k_2 calculated using MESMER. Note that the model reproduces the experimental point at 293 K if it is assumed that there is an equal probability of the reaction proceeding via each HOSiO isomer. In the temperature region above 1200 K relevant to the present study, the reaction should be fast enough to oxidise SiO to SiO_2 in around 40 days. However, reaction 2 is very close to being thermoneutral, and unfortunately the reverse reaction (SiO_2 + H) is about 50 times faster

above 1000 K (Figure 2). SiO and SiO_2 will therefore rapidly reach a steady-state. For instance, in an outflow at 1400 K where the OH/H ratio is 2×10^{-5}, the SiO_2/SiO ratio will be only 3×10^{-6}.

In the absence of OH, the other route to oxidise SiO would be the endothermic reaction

$$SiO + H_2O \rightarrow SiO_2 + H_2 \qquad \Delta H_0 = 50 \text{ kJ mol}^{-1} \qquad (3)$$

However, there is a barrier of 131 kJ mol^{-1} on the PES of this reaction (involving a rearrangement from an intermediate OSi(H)OH to OSiO + H_2), so that this reaction will be extremely slow e.g. $k_3(1400 \text{ K}) = 9 \times 10^{-18}$ cm^3 $molecule^{-1}$ s^{-1}. In any case, the reverse reaction ($SiO_2 + H_2$) has a barrier of only 81 kJ mol^{-1}, and so will be about 3 orders of magnitude faster.

Fortunately, the situation for the oxidation of TiO is rather different. The PES for the OH oxidation reaction

$$TiO + OH \rightarrow TiO_2 + H \qquad \Delta H_0 = -141 \text{ kJ mol}^{-1} \qquad (4)$$

proceeds via a deep well corresponding to HOTiO (bound by 421 kJ mol^{-1} with respect to TiO + OH), which then dissociates without a barrier to the products which lie 141 kJ mol^{-1} below the entrance channel. In this situation, the forward reaction is fast, but the reverse reaction is extremely slow, as shown in Figure 2. The result is that the TiO_2/TiO ratio is around 4% at 1400 K in the outflow, a much more favourable situation. H_2O may also play a role in the oxidation of TiO:

$$TiO + H_2O \rightarrow TiO_2 + H_2 \qquad \Delta H_0 = -85 \text{ kJ mol}^{-1} \qquad (5)$$

However, this reaction does not conserve electronic spin, since ground-state TiO is a triplet (the state is $^3\Delta$) and TiO_2 is a singlet ($^1A_1$). If spin is conserved and triplet TiO_2 formed, the reaction would be endothermic by 245 kJ mol^{-1} and thus negligibly slow. The probability of

spin-hopping from the triplet to singlet may not be negligible if there is a crossing seam between the two PESs. However, for the present model this probability is taken to be zero, so that reaction 4 is assumed to be the only pathway for oxidising TiO.

Formation of the metal titanates and silicates

The next challenge is to oxidise TiO_2 and SiO_2 further. Bimolecular reaction with OH,

$$TiO_2 + OH \rightarrow OTiO_2 + H \qquad \Delta H_0 = 192 \text{ kJ mol}^{-1} \qquad (6)$$

$$SiO_2 + OH \rightarrow OSiO_2 + H \qquad \Delta H_0 = 182 \text{ kJ mol}^{-1} \qquad (7)$$

is too endothermic to be significant. Although recombination is exothermic,

$$TiO_2 + OH (+ M) \rightarrow HOTiO_2 \qquad \Delta H_0 = -319 \text{ kJ mol}^{-1} \qquad (8)$$

$$SiO_2 + OH (+ M) \rightarrow HOSiO_2 \qquad \Delta H_0 = -262 \text{ kJ mol}^{-1} \qquad (9)$$

this route is not promising for three reasons (apart from these recombination reactions being slow because of the low pressure of H_2 (=M) in the outflow). Firstly, the reactions involve recombination with OH which is a very minor species. Secondly, the resulting $HOTiO_2$ and $HOSiO_2$ will not be stable against thermal decomposition, because their bond energies of 319 and 262 kJ mol^{-1} are considerably smaller than the benchmark 400 kJ mol^{-1}. Thirdly, these molecules undergo very exothermic reactions with H, which are likely to be fast:

$$HOTiO_2 + H \rightarrow H_2O + TiO_2 \qquad \Delta H_0 = -174 \text{ kJ mol}^{-1} \qquad (10)$$

$$HOSiO_2 + H \rightarrow H_2O + SiO_2 \qquad \Delta H_0 = -231 \text{ kJ mol}^{-1} \qquad (11)$$

The only viable option appears to be recombination with H_2O:

$$TiO_2 + H_2O (+ M) \rightarrow OTi(OH)_2 \qquad \Delta H_0 = -331 \text{ kJ mol}^{-1} \qquad (12)$$

$$SiO_2 + H_2O (+ M) \rightarrow OSi(OH)_2 \qquad \Delta H_0 = -277 \text{ kJ mol}^{-1} \qquad (13)$$

Figure 3 illustrates the PES for reaction 12. This shows that after initially forming a TiO_2-H_2O complex, rearrangement over a barrier submerged below the energy of the entrance channel leads to the product where three O atoms are now bound to the Ti. MESMER calculations (Table 2) show that reaction 12 is nearly an order of magnitude faster than reaction 13, largely because it is more exothermic. It should be noted that because of the exothermicity, and the large number of low-frequency vibrational modes of $OTi(OH)_2$ (Table 3), the resulting high density of ro-vibrational states means that k_{12} is large enough for this reaction to be viable even at the low pressure of H_2 (=M) in the outflow. Both $OTi(OH)_2$ and $OSi(OH)_2$ are relatively stable with respect to reaction with H:

$$OTi(OH)_2 + H \rightarrow HOTiO + H_2O \qquad \Delta H_0 = 51 \text{ kJ mol}^{-1} \qquad (14)$$

$$OSi(OH)_2 + H \rightarrow HOSiO + H_2O \qquad \Delta H_0 = 36 \text{ kJ mol}^{-1} \qquad (15)$$

However, their bond energies are only 331 and 277 kJ mol^{-1}, respectively, so that thermal dissociation at temperatures above 1000 K will compete with the metal atom reactions discussed below.

Figure 4 shows the PESs for the reactions

$$Ca + OTi(OH)_2 \rightarrow CaTiO_3 + H_2 \qquad \Delta H_0 = -175 \text{ kJ mol}^{-1} \qquad (16)$$

$$Fe + OTi(OH)_2 \rightarrow FeTiO_3 + H_2 \qquad \Delta H_0 = -67 \text{ kJ mol}^{-1} \qquad (17)$$

$$Mg + OTi(OH)_2 \rightarrow MgTiO_3 + H_2 \qquad \Delta H_0 = 5 \text{ kJ mol}^{-1} \qquad (18)$$

All three reactions follow essentially the same mechanism, which is illustrated in Figure 1 for reaction 16. Addition of the Ca atom leads to a $CaTiO_3H_2$ intermediate. This rearranges by migration of one of the H atoms to the Ti, forming the more stable $CaTi(H)O_3H$ intermediate via transition state TS1. $CaTi(H)O_3H$ can in turn rearrange by twisting the hydroxyl H so that H_2 can form, leading via transition state TS2 to the products $CaTiO_3 + H_2$.

Inspection of Figure 4 shows that for reaction 16, TS1 and TS2 are submerged well below the reactant entrance channel, so this reaction will proceed rapidly even at low temperatures. Furthermore, the overall reaction is pretty exothermic, so the reverse reaction rate coefficient must have a large activation energy and the reaction will be relatively slow even at high temperatures. The rate coefficients k_{16} and k_{-16} calculated by MESMER are listed in Table 2. Because of the importance of this reaction, the molecular properties of each of the stationary points on the PES are listed in Table 3.

In contrast to reaction 16, for Fe + $OTi(OH)_2$ the barrier TS1 is no longer submerged (height = 21 kJ mol^{-1}), so k_{17} has a positive activation energy. The reaction is also much less exothermic, so the reverse reaction is much faster (Table 2). For Mg the situation is even worse: TS1 is now 55 kJ mol^{-1} above the Mg + $OTi(OH)_2$ entrance channel and the overall reaction is slightly endothermic.

The PESs for the analogous reactions of Ca, Fe and Mg with $OSi(OH)_2$ have the same topographical features. The relative energies of their respective stationary points are listed in Table 4. This shows that the Ca reaction has submerged barriers and is the most exothermic, whereas there are significant barriers for the Fe and Mg reactions. The resulting rate coefficients for the forward and reverse reactions are also listed in Table 2.

Formation of $CaTiO_3$ clusters

Because of the large number of atoms with relatively high atomic numbers, calculations on the $CaTiO_3$ dimer and trimer were performed only at the B3LYP/6-311+g(2d,p) level of theory. Formation of these species is highly exothermic:

$$CaTiO_3 + CaTiO_3 (+ M) \rightarrow (CaTiO_3)_2 \qquad \Delta H_0 = -458 \text{ kJ mol}^{-1} \qquad (19)$$

$$CaTiO_3 + (CaTiO_3)_2 (+ M) \rightarrow (CaTiO_3)_3 \qquad \Delta H_0 = -478 \text{ kJ mol}^{-1} \qquad (20)$$

The most stable form of the dimer is illustrated at the bottom of Figure 1. Because reaction 19 is well into the fall-off region between third- and second-order kinetics even at the low pressures of a stellar outflow, the MESMER calculations of k_{19} over a range of T and p were fitted to the Lindemann expression modified by a broadening factor F_c [21]:

$$k_{19} = \frac{k_{\mathrm{rec},0}[\mathrm{M}]}{1+\frac{k_{\mathrm{rec},0}[\mathrm{M}]}{k_{\mathrm{rec},\infty}}} F_c^{\ \beta}, \qquad \text{where } \beta = \frac{1}{\left\{1+\left(\log_{10}\left(\frac{k_{\mathrm{rec},0}[\mathrm{M}]}{k_{\mathrm{rec},\infty}}\right)\right)^2\right\}} \qquad \text{(III)}$$

$k_{\mathrm{rec},0}$ and $k_{\mathrm{rec},\infty}$ are the low- and high-pressure limiting rate coefficients, respectively. The fitted values are given in Table 2.

Formation of TiO_2 particles

TiO_2 is able to form a strongly-bound dimer [47], which can then go on to form larger clusters [6]:

$$TiO_2 + TiO_2 (+ M) \rightarrow Ti_2O_4 \qquad \Delta H_0 = -507 \text{ kJ mol}^{-1} \qquad (21)$$

where the enthalpy change at 0 K is taken from a set of very high level theory calculations [47]. Reaction 21 will be in competition with reaction 12, and could therefore constrain the rate of metal titanate formation. The rate coefficients k_{21} and k_{-21} were therefore calculated using MESMER and included in the model (Table 2).

It should be pointed out that mixed titano-silicates ($Ti_xSi_yO_z$) could also form. For instance,

$$TiO_2 + SiO_2 (+M) \rightarrow TiSiO_4 \qquad \Delta H_0 = -480 \text{ kJ mol}^{-1} \qquad (22)$$

Note that the enthalpy change is intermediate between the -408 kJ mol^{-1} for SiO_2 dimerization, and ΔH_0 for TiO_2 dimerization (reaction 21). Although Gail and co-workers [6] have shown that the SiO/SiO_2 system is not effective compared with TiO_2 in forming new particles in an outflow, the mixed system may be more competitive because of the large abundance of SiO_2. However, this complex system is beyond the scope of the present study.

Predicted CN formation in a stellar outflow

The outflow model was now run using the rate coefficients in Table 2. Figure 5 illustrates the concentrations of a variety species over the 1400 days that it takes for the temperature in the outflow to drop from 1500 to 1000 K at a constant outflow velocity of 2 km s^{-1}. The case shown is for a mass loss rate of 4×10^{-5} $M_\odot$ y^{-1}. The concentrations of atomic Ca, Mg and Fe decrease due to the expansion of the outflow. TiO and TiO_2 decay more rapidly because of formation of metal titanates. Note that TiO is in excess over TiO_2 at the highest temperatures, but their concentrations become nearly equal by 1000 K because the equilibrium constant K_4 increases at lower temperatures (due to the exothermicity of reaction 4).

$CaTiO_3$ is the most abundant CN-precursor formed, by more than 3 orders of magnitude over $CaSiO_3$. The Fe and Mg silicates (and titanates) make a negligible contribution to CN formation, which is in agreement with the work of Gail and Sedlmayr [4,9,10]. However, the present model does not support the study of Jeong et al. [6] which concluded that TiO_2 clusters must be the major component of CN in O-rich outflows. Figure 5 shows that the TiO_2 dimer (whose formation would be the first step in forming TiO_2 clusters) is a very minor component. This is because TiO_2 recombines readily with H_2O (reaction 12), and since the H_2O/TiO_2 ratio is greater than 10^5 this reaction is much more likely than recombination of TiO_2 with itself. Hence, the titanium oxides end up as $CaTiO_3$ clusters via reaction 16.

Why is $CaTiO_3$ formation so dominant in this system, even though Ca is 15 times less abundant than Fe and Mg, and TiO is 420 times less abundant than SiO [37]? The reason is that reaction 16 is much faster in the conditions of the outflow than the other five reactions involving these metal atoms reacting with $OTi(OH)_2$ or $OSi(OH)_2$. There are essentially two reasons: 1) the rate coefficient k_{16} is large and has a small T-dependence, and k_{-16} is comparatively small; 2) the TiO_2/TiO ratio is much larger than SiO_2/SiO (see above), and k_{12} is nearly a factor of 10 larger than k_{13}, so that $OTi(OH)_2$ forms much more rapidly than $OSi(OH)_2$ and is then more stable against thermal dissociation.

Figure 6 (top panel) illustrates the particle size distribution in the outflow at T = 1000 K, for a range of mass loss rates from (2 – 10) × 10^{-5} $M_\odot$ y^{-1}. This shows that in all cases there is a large concentration of $CaTiO_3$ monomers in the smallest bin (r = 0.28 nm). Because reaction 19 is not at its high pressure limit at the low pressures in the outflow, k_{19} is about 3 orders of magnitude below the Brownian coagulation rate coefficient. This creates a bottleneck: once the dimer forms, it reacts rapidly with other $CaTiO_3$ polymers (including the monomer) to grow away rapidly to larger particle sizes. For the largest mass loss rate investigated (1 × 10^{-4} $M_\odot$ y^{-1}), there is significant depletion of the monomer by coagulation with the substantial number of larger particles, and the distribution peaks around r = 3 nm, with 2% of particles being larger than 5 nm. In contrast, the distribution for the mass loss rate of 2 × 10^{-5} $M_\odot$ y^{-1} peaks at only 0.55 nm.

If the minimum size of a CN particle is defined (arbitrarily) as r = 2 nm (such a particle would contain ~370 $CaTiO_3$ molecules), then the time evolution of CN particles can be followed in the model. This is shown in Figure 6 (bottom panel), for the same range of mass loss rates. The particle concentration is normalised to the number of H nuclei, as has been done in previous work [6]. The grey line in the figure corresponds to 10^{-13} CN particles per

number of H nuclei. This is typically the mixing ratio of dust grains observed in circumstellar shells, and hence a lower limit to the CN particle number [6]. For these model conditions, this number is exceeded for mass loss rates of 3×10^{-5} $M_{\odot}$ y^{-1} and higher. For mass loss rates of 7×10^{-5} $M_{\odot}$ y^{-1} and higher, sufficient CN particles have been produced while the outflow temperature is still above 1100 K. A final point is that both panels of Figure 6 demonstrate how a variation in the mass loss rate by only a factor of 5 produces huge changes in the particle size distribution and the rate of production of CN particles. This emphasises the highly nonlinear kinetics involved in the gas-phase production of $CaTiO_3$, its dimerisation, and the subsequent growth of CN particles.

In order to compare with previous work on the nucleation rates of CN particles in outflows, the present kinetic model can be used to compute the nucleation rate J_* of particles with $r > 2$ nm, normalised to the total H nucleus concentration (termed $J_*/[\Sigma H]$). Jeong et al. [6] identified a dust formation "window" corresponding to the inner region of dust shells around AGB stars, where the pressure lies in the range 10^{-3} - 0.1 Pa and temperature in the range 1000 – 1200 K. The present model was therefore run at a fixed pressure of 0.01 Pa, and three different temperatures (1000, 1100 or 1200 K) covering this range. The resulting nucleation rates $J_*/[\Sigma H]$ are shown in Figure 7. This illustrates graphically the non-linear effect of temperature on particle production. Note that there is a delay before the CN particles appear, which gets much longer at higher temperatures. This delay is caused by the need to first produce sufficient $CaTiO_3$ for the rate of dimer production, which is second-order in $[CaTiO_3]$, to become fast enough. There is then a further delay while the new $CaTiO_3$ clusters grow to 2 nm. The peak nucleation rates and times are also very sensitive to temperature: at 1000 K, $J_*/[\Sigma H]$ peaks at 5.4×10^{-17} s^{-1} after 35 days, compared with 2.4×10^{-17} s^{-1} after 56 days at 1100 K, and 2×10^{-19} s^{-1} after 300 days at 1200 K. The subsequent decrease in J_* in each case results from the depletion of gas-phase TiO which is required to make $CaTiO_3$. It

has been shown previously [6] that in order to explain the observed dust density in circumstellar shells, the nucleation rate should lie in the range $10^{-22} < J_*/[\Sigma H] < 10^{-14}$ s^{-1}. The $CaTiO_3$ mechanism clearly achieves this.

Conclusions

This study has used a variety of theoretical tools to elucidate a mechanism for producing $CaTiO_3$ molecules from Ca and TiO in the challenging environment of a stellar outflow at temperatures above 1000 K. The mechanism is efficient because it involves two exothermic bimolecular reactions (TiO + OH, and Ca + $OTi(OH)_2$) and only a single recombination reaction ($TiO_2 + H_2O$). The very large dipole moment of $CaTiO_3$ and the stability of its polymeric clusters then favour the rapid formation of CN particles on which silicates can condense as the outflow cools below 1000 K.

This is of course a theoretical study and it would be valuable to test at least some parts of the mechanism experimentally. However, the very properties that should make $CaTiO_3$ an effective particle precursor will also make it extremely difficult to create in the gas phase at large enough concentrations to observe in the laboratory. Finally, although the stellar outflow model used here is quite simplistic, it demonstrates that $CaTiO_3$ should be an outstanding candidate for CN formation. In particular, new particle formation starts to operate at temperatures much higher than the temperatures typically observed at the inner edge of dust shells [48]. Nevertheless, it should be recognised that mass loss rates in excess of 1×10^{-5} $M_\odot$ y^{-1} are required for this mechanism to operate effectively in the model (Figure 6), and this is close to the upper limit of observed mass loss rates around dust-forming stars.

Acknowledgments

This study was supported by project number 291332 (CODITA – Cosmic Dust in the Terrestrial Atmosphere) from the European Research Council. The author thanks Professor Paola Caselli (University of Leeds) and Dr Christiane Helling (University of St. Andrews) for helpful discussions, and acknowledges partial support from EU COST Action CM 0805 – The Chemical Cosmos.

References

1. Gail, H. P., Zhukovska, S. V., Hoppe, P. & Trieloff, M. 2009 Stardust from asymptotic giant branch stars. *Astrophys. J.* 698, 1136-1154.

2. Gail, H. P. & Sedlmayr, E. 1999 Mineral formation in stellar winds - I. Condensation sequence of silicate and iron grains in stationary oxygen rich outflows. *Astronomy and Astrophysics* 347, 594-616.

3. Waters, L., Molster, F. J., deJong, T., Beintema, D. A., Waelkens, C., Boogert, A. C. A., Boxhoorn, D. R., deGraauw, T., Drapatz, S., Feuchtgruber, H., et al. 1996 Mineralogy of oxygen-rich dust shells. *Astronom. Astrophys.* 315, L361-L364.

4. Gail, H. P. & Sedlmayr, E. 1998 Inorganic dust formation in astrophysical environments. *Faraday Discuss.* 109, 303-319.

5. Lagadec, E., Mekarnia, D., Pacheco, J. A. D. & Dougados, C. 2005 Dust temperature and density profiles in the envelopes of AGB and post-AGB carbon stars from mid-infrared observations. *Astronom. Astrophys.* 433, 553-564.

6. Jeong, K. S., Winters, J. M., Le Bertre, T. & Sedlmayr, E. 2003 Self-consistent modeling of the outflow from the O-rich Mira IRC-20197. *Astronom. Astrophys.* 407, 191-206.

7. Sturm, E., Gonzalez-Alfonso, E., Veilleux, S., Fischer, J., Gracia-Carpio, J., Hailey-Dunsheath, S., Contursi, A., Poglitsch, A., Sternberg, A., Davies, R., et al. 2011 Massive molecular outflows and negative feedback in ULIRGS observed by HERSCHEL-PACS. *Astrophys. J. Lett.* 733, 1-5.

8. Keady, J. J., Hall, D. N. B. & Ridgway, S. T. 1988 The IRC + 10216 circumstellar envelope. I. Models for the dust and gas. *Astrophys. J.* 326, 832-842.

9. Gail, H. P. & Sedlmayr, E. 1998 Dust Formation in M Stars. In *The Molecular Astrophysics of Stars and Galaxies* (ed. T. W. Hartquist & D. A. Williams), pp. 285-312. Oxford: Clarendon Press.

10. Gail, H. P. & Sedlmayr, E. 1999 Mineral formation in stellar winds - I. Condensation sequence of silicate and iron grains in stationary oxygen rich outflows. *Astronom. Astrophys.* 347, 594-616.

11. Goumans, T. P. M. & Bromley, S. T. 2012 Efficient nucleation of stardust silicates via heteromolecular homogeneous condensation. *Month. Not. R. Astronom. Soc.* 420, 3344-3349.

12. Paquette, J. A., Ferguson, F. T. & Nuth, J. A., III. 2011 A model of silicate grain nucleation and growth in circumstellar outflows. *Astrophys. J.* 732, Article Number: 62.

13. Donn, B. & Nuth, J. A. 1985 Does nucleation theory apply to the formation of refractory circumstellar grains? *Astrophys. J.* 288, 187-190.

14. Paquette, J. A. & Nuth, J. A., III. 2011 The lack of chemical equilibrium does not preclude the use of classical nucleation theory in circumstellar outflows. *Astrophys. J. Lett.* 737, article no.: L6.

15. Cherchneff, I. & Dwek, E. 2010 The Chemistry of population III supervnova ejecta. II. The nuecleation of molecular clusters as a diagnostic for dust in the early universe. *Astrophys. J.* 713, 1-24.

16. Saunders, R. W. & Plane, J. M. C. 2011 A Photo-Chemical Method for the Production of Olivine Nanoparticles as Cosmic Dust Analogues. *Icarus* 212, 373-382.

17. Saunders, R. W. & Plane, J. M. C. 2006 A laboratory study of meteor smoke analogues: Composition, optical properties and growth kinetics. *J. Atmos. Solar-Terr. Phys.* 68, 2182-2202.

18. Plane, J. M. C. 2011 On the role of metal silicate molecules as ice nuclei. *J. Atmos. Solar-Terr. Phys.* 73, 2192-2200.

19. Rollason, R. J. & Plane, J. M. C. 2000 The reactions of FeO with O_3, H_2, H_2O, O_2 and CO_2. *Phys. Chem. Chem. Phys.* 2, 2335-2343.

20. Rollason, R. J. & Plane, J. M. C. 2001 A kinetic study of the reactions of MgO with H2O, CO2O2: implications for magnesium chemistry in the mesosphere. *Phys. Chem. Chem. Phys.* 3, 4733-4740.

21. Plane, J. M. C. & Rollason, R. J. 2001 Kinetic study of the reactions of CaO with H_2O, CO_2, O_2, and O_3: Implications for calcium chemistry in the mesosphere. *J. Phys. Chem. A* 105, 7047-7056.

22. Foresman, J. B. & Frisch, A. 1996 *Exploring chemistry with electronic structure methods*. Pittsburgh PA: Gaussian, Inc.

23. Montgomery, J. A., Frisch, M. J., Ochterski, J. W. & Petersson, G. A. 2000 A complete basis set model chemistry. VII. Use of the minimum population localization method. *J. Chem. Phys.* 112, 6532-6542.

24. Frisch, M. J., Trucks, G. W., Schlegel, H. B., Scuseria, G. E., Robb, M. A., Cheeseman, J. R., Scalmani, G., Barone, V., Mennucci, B., Petersson, G. A., et al. 2009 *Gaussian 09, Revision A.1*. Wallingford CT: Gaussian, Inc.

25. De Avillez Pereira, R., Baulch, D. L., Pilling, M. J., Robertson, S. H. & Zeng, G. 1997 Pressure and Temperature Dependence of the Multichannel Rate Coefficients for the CH_3 + OH System. *J. Phys. Chem.* 101, 9681.

26. Self, D. E. & Plane, J. M. C. 2003 A kinetic study of the reactions of iron oxides and hydroxides relevant to the chemistry of iron in the upper atmosphere. *Phys. Chem. Chem. Phys.* 5, 1407-1418.

27. Miller, J. A. & Klippenstein, S. J. 2006 Master Equation Methods in Gas Phase Chemical Kinetics. *J. Phys. Chem. A* 110, 10528-10544.

28. Robertson, S. H., Pilling, M. J., Jitariu, L. C. & Hillier, I. H. 2007 Master equation methods for multiple well systems: application to the 1-,2-pentyl system. *Phys. Chem. Chem. Phys.* 9, 4085-97.

29. Glowacki, D. R. & Pilling, M. J. 2010 Unimolecular Reactions of Peroxy Radicals in Atmospheric Chemistry and Combustion. *Chem. Phys. Chem.* 11, 3836-3843.

30. Georgievskii, Y. & Klippenstein, S. J. 2005 Long-range transition state theory. *J. Chem. Phys.* 122, art. no. 194103.

31. Gilbert, R. G. & Smith, S. C. 1990 *Theory of Unimolecular and Recombination Reactions*. Oxford: Blackwell.

32. Robertson, S. H., Glowacki, D. R., Liang, C.-H., Morley, C., Shannon, R., Blitz, M. & Pilling, M. J. MESMER (Master Equation Solver for Multi-Energy Well Reactions), 2008-2012; an object oriented C++ program for carrying out ME calculations and eigenvalue-eigenvector analysis on arbitrary multiple well systems, http: //sourceforge.net/projects/mesmer.

33. Bartis, J. T. & Widom, B. 1974 Stochastic models of the interconversion of three or more chemical species. *J. Chem. Phys.* 60, 3474-82.

34. Press, W. H., Flannery, B. P., Tukolsky, S. A. & Vetterling, W. T. 1986 *Numerical Recipes*. Cambridge: Cambridge University Press.

35. Manion, J. A., Huie, R. E., Levin, R. D., Jr., D. R. B., Orkin, V. L., Tsang, W., McGivern, W. S., Hudgens, J. W., Knyazev, V. D., Atkinson, D. B., et al. NIST Chemical Kinetics Database, NIST Standard Reference Database 17, Version 7.0, Release 1.4.3, Data version 2008.12, web address: http://kinetics.nist.gov/: National Institute of Standards and Technology, Gaithersburg, Maryland.

36. Loup, C., Forveille, T., Omont, A. & Paul, J. F. 1993 CO and HCN observations of cicumstellar envelopes - a catalog of mass-loss rates and distributions. *Astronom. Astrophys. Supplement Ser.* 99, 291-377.

37. Anders, E. & Ebihara, M. 1982 Solar-system abundances of the elements. *Geochim. Cosmochim. Acta* 46, 2363-2380.

38. Asplund, M., Grevesse, N., Sauval, A. J. & Scott, P. 2009 The Chemical Composition of the Sun. In *Annual Review of Astronomy and Astrophysics*, vol. 47 (ed. R. Blandford, J. Kormendy & E. VanDishoeck), pp. 481-522. Palo Alto: Annual Reviews.

39. Fuchs, N. A. 1964 *Mechanics of aerosols*. New York: Macmillan.

40. Saunders, R. W. & Plane, J. M. C. 2010 The formation and growth of Fe2O3 nanoparticles from the photo-oxidation of iron pentacarbonyl. *J. Aerosol Sci.* 41, 475-489.

41. Broadley, S. L. & Plane, J. M. C. 2010 A kinetic study of reactions of calcium-containing molecules with O and H atoms: implications for calcium chemistry in the upper atmosphere. *Phys. Chem. Chem. Phys.* 12, 9095-9107.

42. Sakamoto, S., White, G. J., Kawaguchi, K., Ohishi, M., Usuda, K. S. & Hasegawa, T. 1998 A search for absorption of Mg and Ca compounds in molecular clouds towards Galactic continuum sources. *Mon. Not. R. Astron. Soc.* 301, 872-880.

43. Furuya, R. S., Walmsley, C. M., Nakanishi, K., Schilke, P. & Bachiller, R. 2003 Interferometric observations of FeO towards Sagittarius B2 *Astron. Astrophys.* 409, L21-L24.

44. Jensen, D. E. & Jones, G. A. 1978 Reaction Rate Coefficients for Flame Calculations. *Combust. Flame* 32, 1-34.

45. Chen, Q.-F., Milburn, R. K., Hopkinson, A. C., Bohme, D. K. & Goodings, J. M. 1999 Magnesium chemistry in the gas phase: calculated thermodynamic properties and experimental ion chemistry in H_2-O_2-N_2 flames. *Int. J. Mass Spectrosc.* 184, 153.

46. Gomez Martin, J. C., Blitz, M. A. & Plane, J. M. C. 2009 Kinetic studies of atmospherically relevant silicon chemistry. Part II: silicon monoxide reactions. *Phys. Chem. Chem. Phys.* 11, 10945-10954.

47. Li, S., Hennigan, J. M., Dixon, D. A. & Peterson, K. A. 2009 Accurate thermochemistry for transition metal oxide clusters. *J. Phys. Chem. A* 113, 7861-7877.

48. Groenewegen, M. A. T., Sloan, G. C., Soszynski, I. & Petersen, E. A. 2009 Luminosities and mass-loss rates of SMC and LMC AGB stars and red supergiants. *Astronomy & Astrophysics* 506, 1277-1296.

49. Baulch, D. L., Cobos, C. J., Cox, R. A., Esser, C., Frank, P., Just, T., Kerr, J. A., Pilling, M. J., Troe, J., Walker, R. W., et al. 1992 Evaluated kinetic data for combustion modelling. *J. Phys. Chem. Ref. Data* 21, 411 - 429.

Table 1. Properties of the Ca, Mg and Fe titanate and silicate molecules

Molecule	Dipole moment (Debye)	Dissociation energy (kJ mol^{-1}) [a]
$CaTiO_3$	10.21	585
$CaSiO_3$	14.30	586
$MgTiO_3$	8.35	548
$MgSiO_3$	12.20	546
$FeTiO_3$	5.87	499
$FeSiO_3$	9.54	467

[a] Dissociation to the metal oxide + TiO_2 or SiO_2

Table 2. Reaction scheme for forming gas-phase Ca, Fe and Mg titanate and silicate molecules in the stellar outflow

No.	Reaction	Rate coefficient [a]	$\Delta H_{0\,K}$ [b] kJ mol^{-1}
	Titanium chemistry		
4	$TiO + OH \rightarrow TiO_2 + H$	$1.4 \times 10^{-11} (1000/T)^{0.39}$	-141
-4	$TiO_2 + H \rightarrow TiO + OH$	$5.0 \times 10^{-10} \exp(-15570/T)$	+141
12	$TiO_2 + H_2O + M \rightarrow OTi(OH)_2 + M$	$2.8 \times 10^{-27} (1000/T)^{7.40}$	-331
-12	$OTi(OH)_2 + M \rightarrow TiO_2 + H_2O + M$	$2.4 \times 10^{-7} \exp(-27700)/T)$	+331
16	$Ca + OTi(OH)_2 \rightarrow CaTiO_3 + H_2$	$9.3 \times 10^{-11} (1000/T)^{0.64}$	-175
-16	$CaTiO_3 + H_2 \rightarrow Ca + OTi(OH)_2$	$5.0 \times 10^{-10} \exp(-20090/T)$	+175
19	$CaTiO_3 + CaTiO_3 + M \rightarrow (CaTiO_3)_2 + M$	$k_{rec,0} = 5.1 \times 10^{-24} (1000/T)^{14.0}$ $k_{rec,\infty} = 6.3 \times 10^{-10} (1000/T)^{0.17}$ $F_c = 0.6$ (see eqn. III)	-458 [c]
-19	$(CaTiO_3)_2 + M \rightarrow CaTiO_3 + CaTiO_3 + M$	$k_{4a} / (1.3 \times 10^{-27} \exp(51705 / T))$	+458 [c]
17	$Fe + OTi(OH)_2 \rightarrow FeTiO_3 + H_2$	$5.4 \times 10^{-11} \exp(-3700/T)$	-67
-17	$FeTiO_3 + H_2 \rightarrow Fe + OTi(OH)_2$	$1.6 \times 10^{-10} \exp(-10040/T)$	+67
18	$Mg + OTi(OH)_2 \rightarrow MgTiO_3 + H_2$	$4.7 \times 10^{-12} \exp(-7340/T)$	+5
-18	$MgTiO_3 + H_2 \rightarrow Mg + OTi(OH)_2$	$3.6 \times 10^{-11} \exp(-6630/T)$	-5
21	$TiO_2 + TiO_2 + M \rightarrow Ti_2O_4 + M$	$8.0 \times 10^{-27} (1000/T)^{6.46}$	-507 [d]
-21	$Ti_2O_4 + M \rightarrow TiO_2 + TiO_2 + M$	$1.4 \times 10^{-4} \exp(-48870/T)$	+507 [d]
	Silicon chemistry		
2	$SiO + OH \rightarrow SiO_2 + H$	$9.6 \times 10^{-13}\ 10^{(5.94e\text{-}4\ T)}$ [e]	-6.4
-2	$SiO_2 + H \rightarrow SiO + OH$	$1.2 \times 10^{-10}\ 10^{(4.57e\text{-}4\ T)}$ [e]	+6.4
13	$SiO_2 + H_2O + M \rightarrow OSi(OH)_2$	$4.0 \times 10^{-28} (1000/T)^{7.68}$	-277
-13	$OSi(OH)_2 + M \rightarrow SiO_2 + H_2O + M$	$8.7 \times 10^{-8} \exp(-22170/T)$	+277
21	$Ca + OSi(OH)_2 \rightarrow CaSiO_3 + H_2$	$2.8 \times 10^{-10} (1000/T)^{0.28}$	-230
-21	$CaSiO_3 + H_2 \rightarrow Ca + OSi(OH)_2$	$3.5 \times 10^{-10} \exp(-26590/T)$	+230
22	$Fe + OSi(OH)_2 \rightarrow FeSiO_3 + H_2$	$7.0 \times 10^{-11} \exp(-5550/T)$	-89
-22	$FeSiO_3 + H_2 \rightarrow Fe + OSi(OH)_2$	$4.8 \times 10^{-11} \exp(-15870/T)$	+89
23	$Mg + OSi(OH)_2 \rightarrow MgSiO_3 + H_2$	$5.4 \times 10^{-12} \exp(-7560/T)$	-48
-23	$MgSiO_3 + H_2 \rightarrow Mg + OSi(OH)_2$	$1.3 \times 10^{-11} \exp(-12040/T)$	+48
	Odd hydrogen chemistry		

24	$OH + H_2 \rightarrow H_2O + H$	$1.6 \times 10^{-12} (T/298)^{1.6} \exp(-160/T)$ [f]	+67
-24	$H_2O + H \rightarrow OH + H_2$	$6.8 \times 10^{-12} (T/298)^{1.6} \exp(-9720/T)$ [f]	-67

[a] Units: bimolecular, cm^3 $molecule^{-1}$ s^{-1}; termolecular, cm^6 $molecule^{-2}$ s^{-1} ; [b] Calculated at the CBS-Q level of theory except where indicated; [c] Calculated at the B3LYP/6-311+g(2d,p) level of theory; [d] Calculated at the CCSD(T)-DK level of theory [47]; [e] Parameterised fit between 900 and 1500 K; [f] Baulch et al. [49].

Table 3. Molecular properties and relative energies of the stationary points on the potential energy surface for Ca + $OTi(OH)_2 \rightarrow CaTiO_3 + H_2$

Molecule	Rotational constants (GHz)	Vibrational frequencies (cm^{-1})	Relative energy ($kJ\ mol^{-1}$)
$OTi(OH)_2$	7.53, 5.23, 3.09	57, 194, 231, 510, 513, 515, 531, 674, 781, 1054, 3882, 3885	0
$CaTiO_3H_2$	6.89, 1.52, 1.29	49, 124, 134, 272, 281, 337, 353, 357, 416, 538, 640, 713, 809, 3882, 3935	-209
TS1	8.23, 1.54, 1.31	1396 *i*, 78, 145, 175, 257, 326, 349, 363, 495, 658, 707, 736, 791, 1398, 3942	-110
$CaTi(H)O_3H$	6.86, 1.63, 1.47	86, 171, 187, 269, 373, 402, 419, 537, 544, 599, 712, 732, 811, 1641, 3924	-305
TS2	8.89, 1.97, 1.68	1291 *i*, 129, 258, 371, 394, 487, 493, 623, 758, 832, 898, 1121, 1173, 1820, 2043	-173
$CaTiO_3$	6.84, 1.84, 1.63	103, 256, 301, 375, 407, 593, 680, 746, 980	-176

Table 4. Energies of the stationary points on the potential energy surfaces of Ca, Fe and Mg with $OSi(OH)_2$, relative to the reactants (Mt = Ca, Fe or Mg).

Reaction	$MtSiO_3H_2$	TS1	$MtSi(H)O_3H$	TS2	$MtSiO_3 + H_2$
$Ca + OSi(OH)_2$	-180	-81	-367	-149	-230
$Fe + OSi(OH)_2$	-157	31	-252	-12	-89
$Mg + OSi(OH)_2$	-87	51	-192	33	-48

Figure Captions

Figure 1. Reaction pathway to form $CaTiO_3$ and the $CaTiO_3$ dimer from Ca and TiO. The geometries are optimised at the B3LYP/6-311+g(2d,p) level of theory.

Figure 2. Temperature-dependent rate coefficients for the reactions SiO + OH $\rightarrow$ SiO_2 + H and TiO + OH $\rightarrow$ TiO_2 + H and their reverse reactions, calculated using the MESMER code (see text). The experimental measurement of SiO + OH from Gomez Martin et al. [46] is shown for comparison.

Figure 3. Potential energy surface calculated at the CBS-Q level of theory for the recombination of TiO_2 and H_2O.

Figure 4. Potential energy surfaces for the reactions of Ca, Fe and Mg with $OTi(OH)_2$, calculated at the CBS-Q level of theory. For the Ca reaction, the intermediates and two transition states (TS1 and TS2) are illustrated in Figure 1.

Figure 5. Modelled evolution of dust condensation nucleus precursors of Ca (dark blue lines), Fe (black lines), Mg (green lines, note the $MgSiO_3$ concentration is too small to appear) and TiO (azure blue lines) in a stationary stellar outflow of 4×10^{-5} $M_\odot$ y^{-1} and fixed velocity of 2 km s^{-1}. Temperature (red line) is shown on the right-hand ordinate axis.

Figure 6. Top panel: modelled size distribution of $CaTiO_3$ particles for a range of mass loss rates, shown at the point when the stellar outflow has cooled to 1000 K and these particles can start to act as condensation nuclei for less refractory gas-phase species. Bottom panel: modelled time evolution of $CaTiO_3$ particles with radii greater than 2 nm (normalised to the H nucleus concentration) during the 1400 days that the outflow cools from 1500 to 1000 K (for the same range of mass loss rates as the top panel). Temperature is shown on the right-

hand ordinate. The horizontal grey line marks the lower limit to the CN particle mixing ratio required to account the observed dust grain density in circumstellar shells [6].

Figure 7. The nucleation rate of particles (r > 2 nm) as a function of time. The rate is normalised to the H nucleus concentration. Each model run is at a constant pressure (0.01 Pa) and temperature (1000, 1100 or 1200 K).

Short title: Dust nucleation

Figure 1.

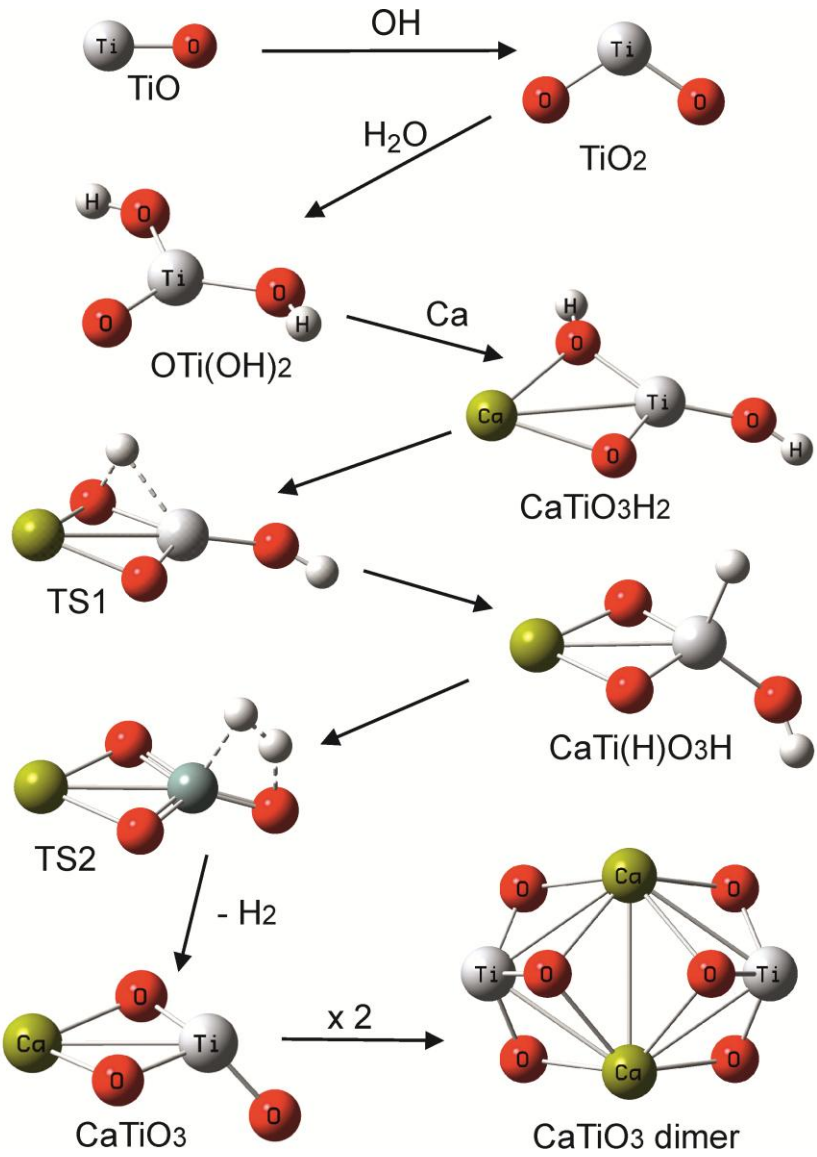

Figure 1. Reaction pathway to form $CaTiO_3$ and the $CaTiO_3$ dimer from Ca and TiO. The geometries are optimised at the B3LYP/6-311+g(2d,p) level of theory.

Figure 2.

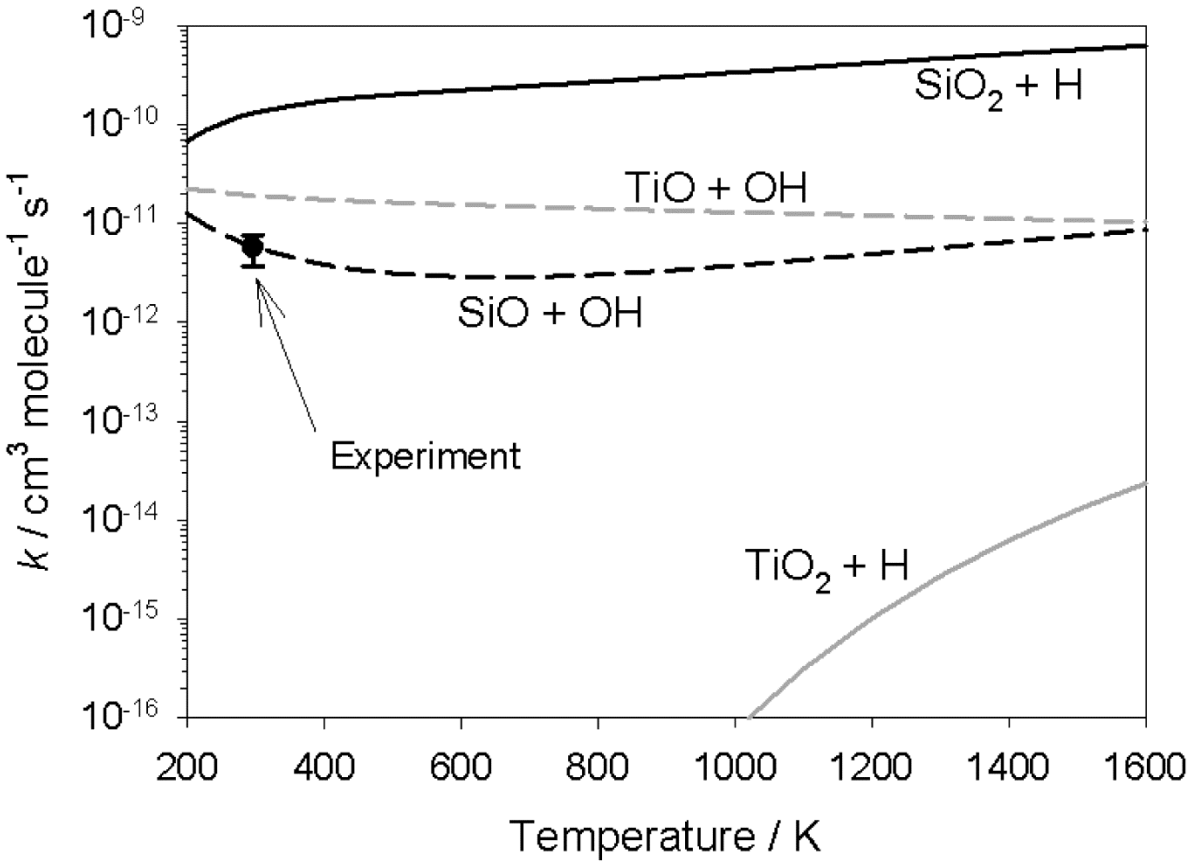

Figure 2. Temperature-dependent rate coefficients for the reactions SiO + OH → SiO_2 + H and TiO + OH → TiO_2 + H and their reverse reactions, calculated using the MESMER code (see text). The experimental measurement of SiO + OH from Gomez Martin et al. [45] is shown for comparison.

Figure 3.

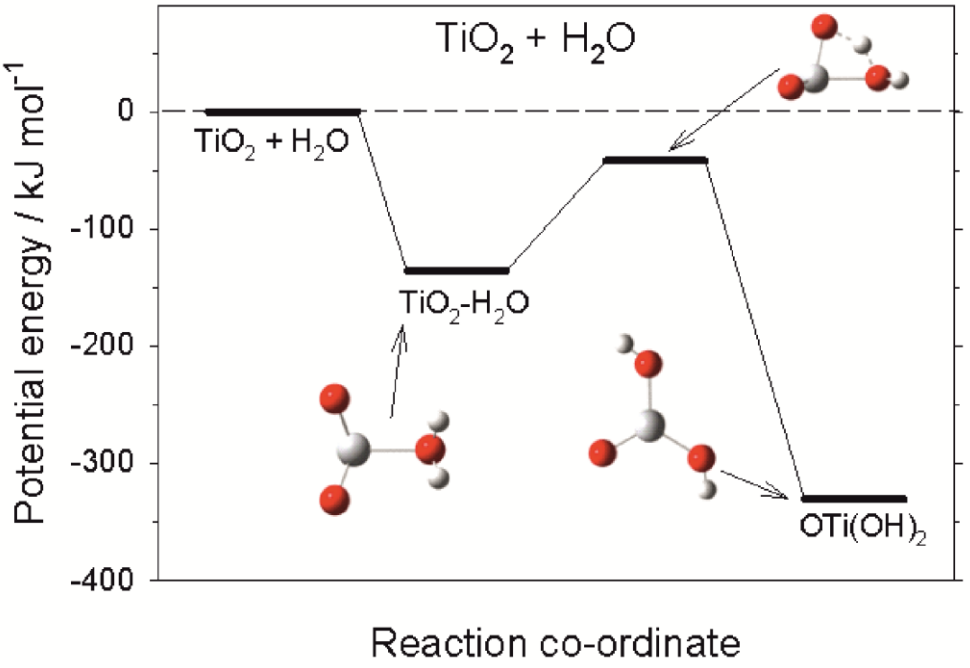

Figure 3. Potential energy surface calculated at the CBS-Q level of theory for the recombination of TiO_2 and H_2O.

Figure 4.

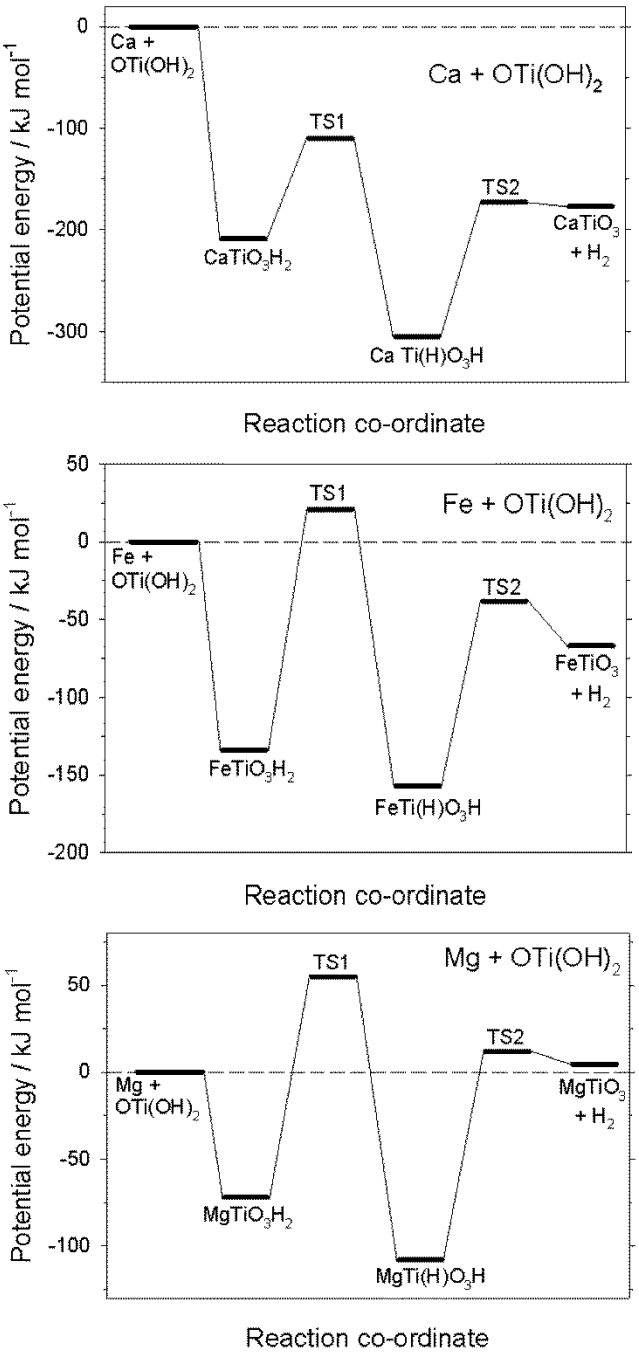

Figure 4. Potential energy surfaces for the reactions of Ca, Fe and Mg with $OTi(OH)_2$, calculated at the CBS-Q level of theory. For the Ca reaction, the intermediates and two transition states (TS1 and TS2) are illustrated in Figure 1.

Figure 5.

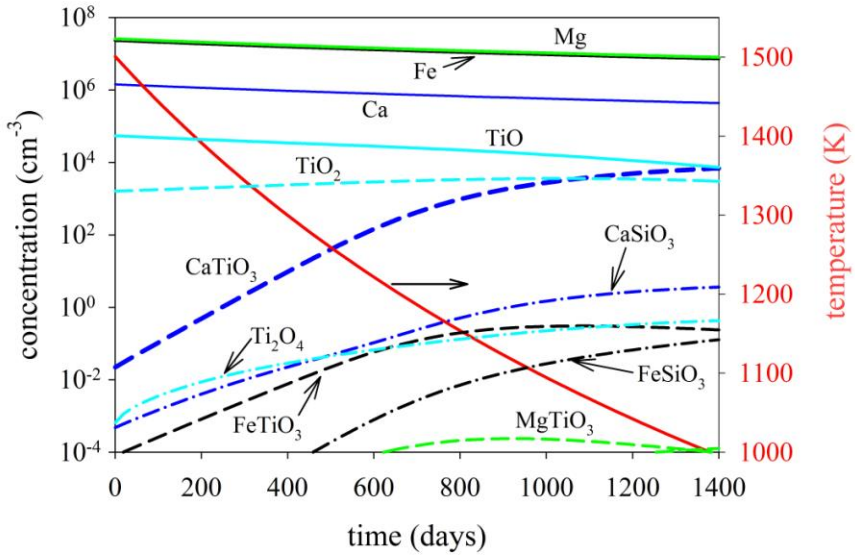

Figure 5. Modelled evolution of dust condensation nucleus precursors of Ca (dark blue lines), Fe (black lines), Mg (green lines, the $MgSiO_3$ concentration is too small to appear) and TiO

(azure blue lines) in a stationary stellar outflow of 4×10^{-5} $M_{\odot}$ y^{-1} and fixed velocity of 2 km s^{-1}. Temperature (red line) is shown on the right-hand ordinate axis.

Figure 6.

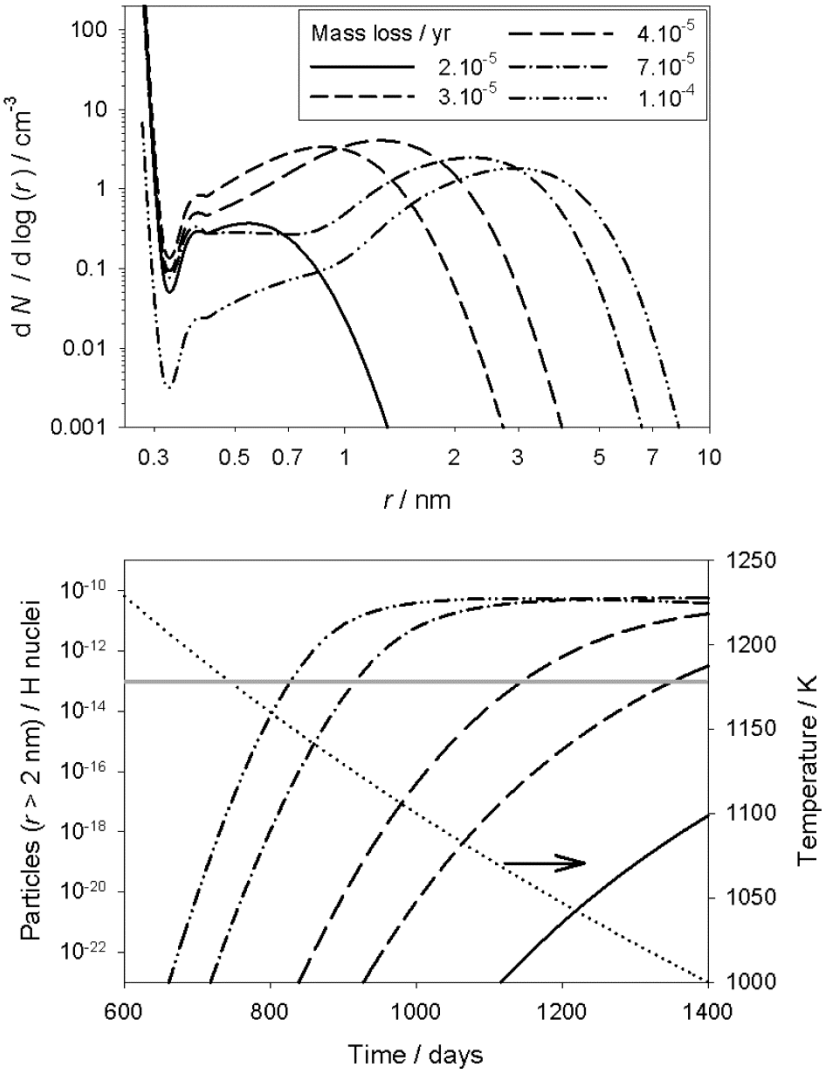

Figure 6. Top panel: modelled size distribution of $CaTiO_3$ particles for a range of mass loss rates, shown at the point when the stellar outflow has cooled to 1000 K and these particles can start to act as condensation nuclei for less refractory gas-phase species. Bottom panel: modelled time evolution of $CaTiO_3$ particles with radii greater than 2 nm (normalised to the H nucleus concentration) during the 1400 days that the outflow cools from 1500 to 1000 K (for the same range of mass loss rates as the top panel). Temperature is shown on the right-hand ordinate. The horizontal grey line marks the lower limit to the CN particle mixing ratio required to account the observed dust grain density in circumstellar shells [6].

Figure 7.

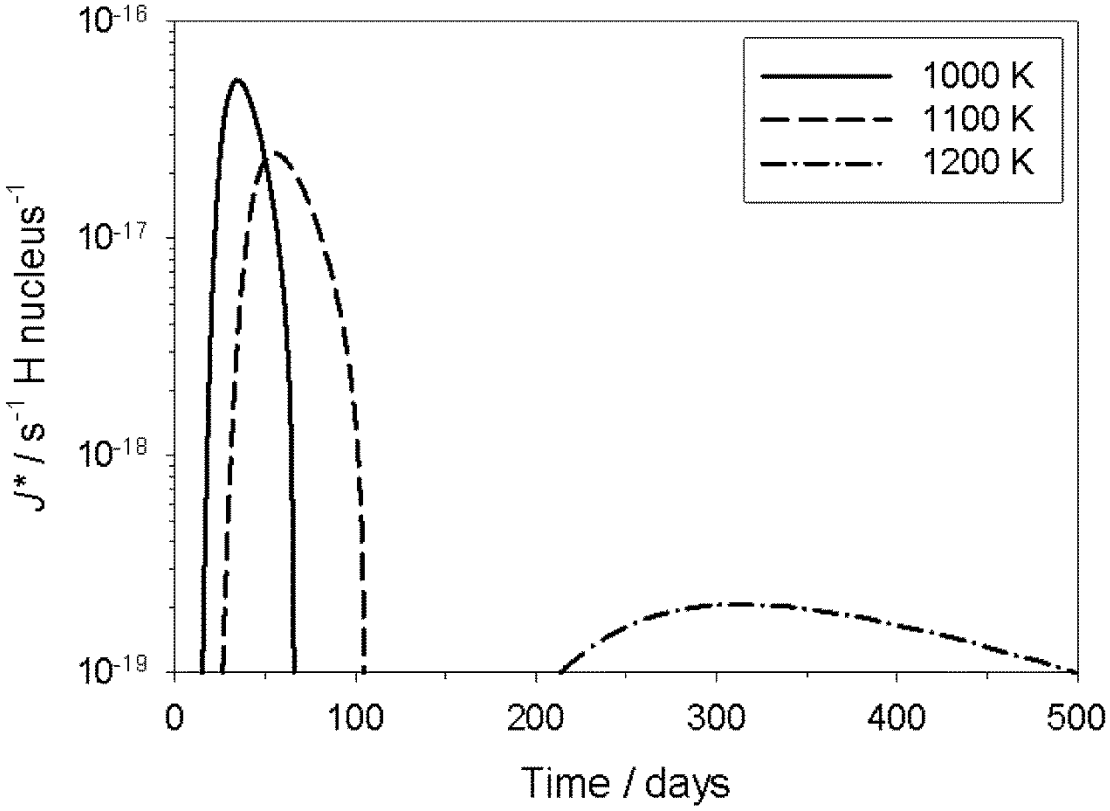

Figure 7. The nucleation rate of particles (r > 2 nm) as a function of time. The rate is normalised to the H nucleus concentration. Each model run is at a constant pressure (0.01 Pa) and temperature (1000, 1100 or 1200 K).